Proceedings of the ASME 2009 Fluids Engineering Division Summer Meeting
FEDSM2009
August 2-6, 2009, Vail, Colorado USA

FEDSM2009-78212

AN EQUATION OF MOTION FOR PARTICLES OF FINITE REYNOLDS NUMBER AND FINITE SIZE

Eric Loth
Department of Aerospace Engineering
University of Illinois at Urbana-Champaign
Urbana, Illinois 61801
Email: loth@illinois.edu

Andrew J. Dorgan
Department of Aerospace Engineering
University of Illinois at Urbana-Champaign
Urbana, Illinois 61801

ABSTRACT

In order to simulate the motion of bubbles, drops, and particles, it is often important to consider finite Reynolds number effects on drag, lift, torque and history force. Herein, an equation of motion is developed for spherical particles with a no-slip surface based on theoretical analysis, experimental data and surface-resolved simulations. The equation of motion is then extended to account for finite particle size. This extension is critical for particles which will have a size significantly larger than the grid cell size, particularly important for bubbles and low-density particles. The extension to finite particle size is accomplished through spatial-averaging (both volume-based and surface-based) of the continuous flow properties. This averaging is consistent with the Faxen limit for solid spheres at small Reynolds numbers and added mass and fluid stress forces at inviscid limits. The finite Re_p corrections are shown to have good agreements with experiments and resolved-surface simulations. The finite size corrections are generally fourth-order accurate and an order of magnitude more accurate than point-force expressions (which neglect quadratic and higher spatial gradients) for particles with size on the order of the gradient length-scales. However, further work is needed for more quantitative assessment of the truncation terms and the overall model robustness and accuracy in complex flows.

Introduction

The motion of particles, drops, and bubbles immersed in a fluid is important in many engineering problems. In aerospace, solid particles or droplets are commonly encountered mixed with a gaseous phase. Air breathing propulsion systems can have important multiphase interactions during all phases of the engine cycle. For example, particles can be ingested during near-ground operation which erode the compressor blades. Ingested water droplets may freeze on the compressor and degrade its performance or cause damage to the engine. The characteristics of fuel sprays and fuel-air mixing in the combustor are important to the efficiency of the engine and generation/concentration of soot particles in the exhaust stream. As a matter of aircraft safety, multiphase interactions are important to the problem of aircraft icing where ice accretion can disrupt the aerodynamic performance of lifting structures.

In environmental science, particles and droplets in the atmosphere can have a substantial impact on weather and environmental safety. Sediment transport in natural bodies of water can play a significant role in the health and maintenance of rivers and coastal areas. For example, silting can dramatically reduce the capacity of rivers and has been cited as one of the reasons for some of the more devastating floods in Asia and elsewhere. Coastal land erosion is another problem that has become more severe in the last few decades since it can lead to substantial losses of animal habitats and affect human population centers. Bubbles are injected in plumes for reservoirs and waste water treatments to increase oxygen content and control pH levels.

Dispersed multiphase numerical techniques are being used to understand these overall processes by following the particles along Lagrangian paths with an equation of motion. Generally, such equations require acceleration terms and these typically correspond to particles of significant Reynolds number and finite

size with respect to flow scales (and grid size). A direct theoretical equation of motion is not available for these conditions. Therefore, the goal of this study is to construct an equation of motion which is appropriate for modeling particles, drops, and bubbles when they have both finite size and finite Reynolds numbers.

Surface force decomposition

The dynamic motion of a particle is described by equating the product of mass and acceleration with the sum of the external forces acting on the particle, e.g.

$$m_p \frac{d\vec{V}_p}{dt} = \vec{F}_{surf} + \vec{F}_g \tag{1}$$

where m_p is the particle mass, $\vec{V}_p$ is the three-dimensional particle velocity, $\vec{F}_{surf}$ is the net force induced by pressure and shear stresses imposed by the continuous phase on the particle surface, and $\vec{F}_g$ is the particle body force induced by the gravitational field. For a particle of homogeneous density, the mass and body force can be written in terms of the particle volume, $\forall_p$, such that $m_p = \rho_p \forall_p$ and $\vec{F}_g = \rho_p \forall_p \vec{g}$ where ρ_p is the particle density and $\vec{g}$ is the gravity vector. While these expressions are simple to employ in a multiphase calculation, $\vec{F}_{surf}$ has been the subject of much research and must be handled carefully to properly model a multiphase interaction. In simulating a large number of particles, it is typically impractical to discretize and resolve the detailed flow around each particle's surface, especially at finite Reynolds numbers. Therefore, a decomposition approach is typically employed to generate $\vec{F}_{surf}$.

In its conventional construction, the "point-force" approximation assumes the particle is sufficiently small compared to the local length scale of the fluid structures such that it is reasonable to use the continuous-phase properties at a single point in space (corresponding to particle center of mass) to describe the force on the particle. In particular, $\vec{F}_{surf}$ can be represented as a linear combination of specific independent forces such that,

$$\vec{F}_{surf} = \vec{F}_D + \vec{F}_L + \vec{F}_{AM} + \vec{F}_{SG} + \vec{F}_H \tag{2}$$

where $\vec{F}_D$ is the quasi-steady-state drag force, $\vec{F}_L$ is the lift force generated by rotation of the particle and fluid shear, $\vec{F}_{AM}$ is the so-called added, or virtual, mass force which accounts for the work required to change the momentum of the surrounding fluid as the particle accelerates, $\vec{F}_{SG}$ is the fluid stress gradient force which accounts for forces that would exist in the absence of the particle due to acceleration of the continuum and the hydrostatic pressure gradient, and finally, $\vec{F}_H$ is the unsteady-drag force or "history" force which accounts for the temporal development of the viscous region in the vicinity of the particle.

Maxey-Riley (MR) and Auton-Hunt-Prud'homme (AHP) Point-Force Expressions

The description of $\vec{F}_{surf}$ as a summation of distinct forces is generally empirical except for some limiting cases which permit a fully theoretical solution for a spherical particle. These solutions are often related to the continuous-phase properties extrapolated to the particle centroid ($\vec{x}_p$), in the absence of the particle's influence; an assumption appropriate when particle length-scales are much smaller than flow gradient length-scales. In this situation, the particle Reynolds number can be defined as

$$Re_p = \frac{\rho_f d_p \|\vec{V}_{rel}\|}{\mu} \tag{3}$$

$$\vec{V}_{rel} = \vec{V}_p - \vec{V}_{f,@p} \tag{4}$$

where μ is the molecular viscosity of the fluid, ρ_f is the fluid density and d_p is the particle diameter which is related to its volume by $d_p = \sqrt[3]{6\forall_p/\pi}$. Additionally, $\vec{V}_f$ represents the fluid velocity and the subscript $_{@p}$ implies the fluid velocity is at $\vec{x} = \vec{x}_p$. There are many such analytical solutions (starting from the seminal work of Stokes in 1851 [1]) which generally assume *a)*inviscid flow conditions ($\mu = 0$) or *b)*creeping flow conditions ($Re_p \to 0$).

Two particularly important theoretical particle equations of motion are the Maxey-Riley (MR) equation for creeping irrotational flow and the Auton-Hunt-Prud'homme (AHP) equation for inviscid rotational flow. These two equations often serve as baseline equations of motion to which additional effects are incorporated. The Maxey-Riley equation [2] assumes a non-rotating, rigid, spherical particle of constant diameter in an unsteady, non-uniform incompressible flow with weak spatial gradients and is limited to $Re_p \ll 1$.

The MR equation of motion yields a decomposition of surfaces forces given by:

$$\vec{F}_D = -3\pi\mu d_p \vec{W} \tag{5}$$

$$\vec{F}_{SG} = \rho_f \forall_p \left(\frac{D\vec{V}_{f,@p}}{Dt} - \vec{g} \right) \tag{6}$$

$$\vec{F}_{AM} = -\rho_f \forall_p C_M \frac{d}{dt} \left(\vec{V}_{rel} - \frac{d_p^2}{40} \nabla^2 \vec{V}_{f,@p} \right) \tag{7}$$

$$\vec{F}_H = -3\pi\mu d_p \left[\int_0^t K(\tau) \frac{d\vec{W}}{d\tau} d\tau + K(0)\vec{W}(0) \right] \tag{8}$$

$$\vec{W} = \vec{V}_{rel} - \frac{d_p^2}{24} \nabla^2 \vec{V}_{f,@p} \tag{9}$$

$$K_{Basset} = \left[\frac{d_p^2}{4\pi\nu(t-\tau)} \right]^{1/2} \tag{10}$$

The original Maxey-Riley derivation assumed $\vec{W}$ is zero at $t = 0$, but the contribution for finite $\vec{W}(0)$ has been included here based on later work by Maxey [3]. At creeping conditions, the effect of linear variation of the flowfield was found to be negligible (hence no lift force due to fluid shear) but curvature of the velocity field does contribute to the surface forces. The corrections associated with this curvature (the ∇^2 terms) are often called Faxen terms, since Faxen [4] was first to obtain such contributions.

Auton [5] and Auton *et al.*[6] considered a much different limit for the continuous-phase: a sphere moving relative to an inviscid fluid such that $\vec{F}_D = \vec{F}_H = \vec{0}$. These studies assumed that the particle was fixed, subjected to a far-field linear shear flow, and that the spatial velocity gradient was weak compared to change in relative velocity across the particle. To extend this to unsteady and straining flows, Auton *et al.*[6] additionally assumed that the temporal velocity gradient was weak.

Auton's derivation leads to the following surface forces

$$\vec{F}_{SG} = \rho_f \forall_p \left(\frac{D\vec{V}_{f,@p}}{Dt} - \vec{g} \right) \tag{11}$$

$$\vec{F}_{AM} = \frac{\rho_f \forall_p}{2} \left(\frac{D\vec{V}_{f,@p}}{Dt} - \frac{d\vec{V}_p}{dt} \right) \tag{12}$$

$$\vec{F}_L = \frac{1}{2} \rho_f \forall_p C_L \left(\vec{V}_{rel} \times \vec{\omega}_{shear} \right) \tag{13}$$

where $\vec{\omega}_{shear} = \vec{V}_{rel}/d_p$. Note the different derivatives in Eq. 12: D/Dt denotes derivatives taken along the fluid path, and d/dt denotes a derivative along the particle path.

It is interesting to compare the AHP equation to the Maxey-Riley equation. We first note that the fluid stress is the same in both cases, so that one may expect it to be generally applicable for spherical particles. The added mass terms are slightly different between Eq. 7 and 12, though Maxey [3] noted that the differences are negligible. For finite Re_p conditions with spherical particles, there have been several experimental and numerical studies [7, 8, 9, 10, 11, 12, 13] which have investigated the added mass force. These studies all showed that that the AHP expression for the added mass force is remarkably reasonable for a wide variety of Re_p values for both solid and fluid particles. They also demonstrated that the empirical (and often used) form proposed by Odar & Hamilton [14] is incorrect, due to their incorrect interpretation of the history forces.

Surface forces for particles at arbitrary Reynolds numbers

In this section, surface forces appropriate for the simulation of particles at arbitrary Reynolds number are developed and discussed. The intent of this section is to "bridge the gap" between the Maxey-Riley equation for creeping flow conditions and the Auton-Hunt-Prud'homme equation for inviscid conditions. As noted in the discussion above, the added mass and fluid stress forces given by Eqs. 11 & 12 are generally accepted for a wide range of Reynolds numbers within the point-force limitations [9, 13]. The quasi-steady drag force can also be given with a commonly accepted form and is disucssed in Section . Expressions for the torque-free lift and history force at finite Reynolds numbers are also put forth in Sections and . Note that a spherical no-slip surface is assumed which is reasonable for solid partilces and contaminated bubbles so long as the combination of Reynolds number and Weber number is moderate [15].

Quasi-steady drag force

The quasi-steady drag force ($\vec{F}_D$ in Eq. 2) arises from the pressure and viscous stresses applied to the particle surface when the particle is subjected to a constant, spatially uniform fluid velocity. The drag force resists relative velocity and is therefore defined to act in the direction opposite of the particle relative velocity, e.g.

$$\vec{F}_D = -\frac{1}{2} \rho_f \|\vec{V}_{rel}\| \vec{V}_{rel} A_p C_D \tag{14}$$

where A_p is the projected area of the particle with value $\pi d_p^2/4$ for a sphere, and C_D is the particle drag coefficient which is a function of particle Reynolds number. For intermediate particle Reynolds numbers ($0.1 < Re_p < 1{,}000$), the flowfield in the rear of the particle undergoes several transitions: from an attached laminar wake, to a separated but still laminar wake, to an unsteady wake. In these Reynolds number regimes and beyond there is no analytical solution available from which one can extract the sphere's drag. In these cases it is common to write the drag coefficient based on [16] as

$$C_D = \frac{24}{Re_p} \left(1.0 + 0.15 Re_p^{0.687} \right) \tag{15}$$

This reverts to Eq. 5 in the limit of $Re_p \ll 1$ and uniform flow. Note that no Faxen-type correction has been proposed to the authors' knowledge for finite Re_p point-force expressions.

History force

The history force accounts for the unsteady component of the drag force which is generated by the temporal development of the viscous region in the vicinity of the particle. As such the force decays in time provided the particle reaches a constant velocity (e.g. terminal velocity in a quiescent fluid). This decay rate is a function of Reynolds number (see Figure 1 for an illustration) and has received attention from a number of researchers.

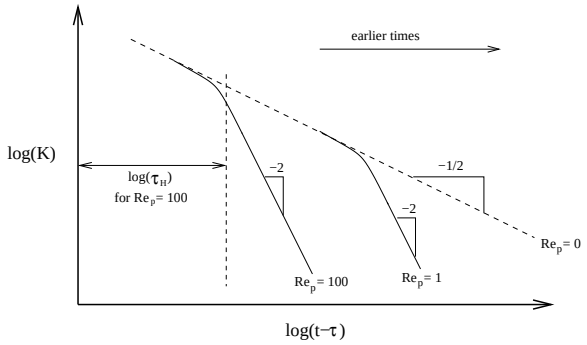

Figure 1. Schematic of history kernel as a function time, where short-times give creeping flow response but long-times result in faster decays. The window model limit of integration is shown for $Re_p = 100$.

The basic form of the history force for a uniform flow is given by

$$\vec{F}_H = 3\pi\mu_f d_p \int_{-\infty}^{t} K(t-\tau)\frac{d\vec{V}_{rel}}{d\tau}d\tau \tag{16}$$

which is the same as given by [2]. Researchers have proposed a number of expressions for the kernel, K, which range from the analytically creeping flow expression given by Basset [17]

$$K_{Basset}(t-\tau) = \left[\frac{4\pi\nu(t-\tau)}{d_p^2}\right]^{-1/2} \tag{17}$$

to the finite Reynolds number from proposed by Mei & Adrian [18]

$$K(t-\tau) = \left(\left[\frac{4\pi\nu(t-\tau)}{d_p^2}\right]^{1/2c_1} + \left[\frac{\pi(t-\tau)^2}{f_H\tau_d}Re_p^3\right]^{1/c_1}\right)^{-c_1} \tag{18}$$

where τ_d is a diffusive time-scale and f_H is a function of Reynolds number,

$$\tau_d = \frac{d_p^2}{\nu} \tag{19}$$

$$f_H = (0.75 + c_2 Re_p)^3 \tag{20}$$

The constants c_1 and c_2 are chosen empirically and have a range of values in the literature. Mei & Adrian [18] chose $c_1 = 2$ and $c_2 = 0.105$, though Dorgan & Loth [19] reviewed a large set of

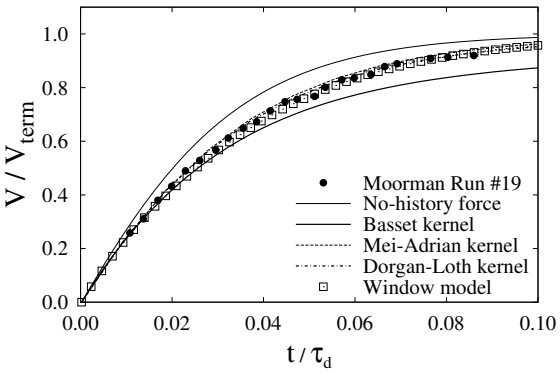

Figure 2. Velocity of particle accelerating to terminal velocity based on experiments of [20] at $Re_{p,term} = 166$ and a density ratio of 3.69 as well predictions with various history force models.

experimental data and found that $c_1 = 2.5$ and $c_2 = 0.2$ provide slightly better predictions, e.g. Figure 2.

The key numerical problem associated with including the history force in a many-particle simulation is the large CPU-time required to evaluate the integral in Eq. 16. In this regard, Dorgan & Loth [19] show that a history force kernel in the form given by Eq. 18 can be approximated with as window-based approach to alleviate much of this CPU overhead. This approach equates two integrals: one using the Basset kernel integrated back for only a portion of the particle lifetime and one using the finite Reynolds number kernel integrated over the entire particle lifetime, i.e.

$$\int_{t-\tau_H}^{t} K_{Basset}(t-\tau)d\tau = \int_0^t K(t-\tau)d\tau \tag{21}$$

The objective is to solve for the non-dimensional "history time", τ_H, appearing in the lower limit of the first integral. Equating the two integrals for $t \to \infty$ allows τ_H to be specified for a particular Re_p and τ_d. For $c_1 = 2.5$ and $c_2 = 0.2$, this history time is well described for $Re_p < 1000$ by [19]:

$$\tau_H = \tau_d\left(\frac{0.502}{Re_p} + 0.123\right)^2 \tag{22}$$

This allows the history force integral to be expressed as

$$\int_{t-t_{window}}^{t} K_{Basset}(t-\tau)d\tau \tag{23}$$

where the lower limit of integration is given by

$$t - t_{window} = \min(0, t-\tau_H) \tag{24}$$

such that a form applicable to both creeping flow and finite Reynolds number is obtained. Note that the window model will predict exactly the same history force as that predicted using the chosen K under the conditions of constant relative acceleration ($dV_{rel}/d\tau$). When the changes in acceleration are appreciable (i.e. appreciable "jerk") the window model will break-down but otherwise this model leads to an order of magnitude or more decrease in CPU-time [19].

Lift force

The lift force is one of the more difficult forces to properly model as there are a number of physical phenomena that lead to the generation of lift; the two primary mechanisms being vorticity in the continuous-phase and rotation of the particle. A special case that combines these two effects is that of "free-rotation" where there is zero torque on the particle, a result achieved when the particle attains an equilibrium spin rate related to the imposed shear. For particles with sufficiently small inertia (e.g. gas bubbles), the equilibrium spin rate is quickly realized such that one may often treat the particle as being in *constant equilibrium*. In all these cases, the magnitude of the vorticity or the spin rate is typically expressed in terms of ω^* and Ω_p^*, which are proportional to the velocity gradient across the particle normalized by the particle's relative velocity, e.g.

$$\omega^* = \frac{\|\vec{\omega}\| d_p}{\|\vec{V_{rel}}\|} \tag{25}$$

$$\Omega_p^* = \frac{\|\vec{\Omega}_p\| d_p}{\|\vec{V_{rel}}\|} \tag{26}$$

where $\vec{\omega}$ is the fluid vorticity and $\vec{\Omega}_p$ is the particle angular velocity. The magnitude of the lift force is typically expressed as a "lift-coefficient" non-dimensionalized in the same manner as Eq. 14:

$$C_L = \frac{\|\vec{F_L}\|}{\frac{\pi}{8}\rho_f \vec{V_{rel}} \cdot \vec{V_{rel}} d_p^2} \tag{27}$$

The direction of the lift is defined to be perpendicular to $\vec{V}_{rel}$ and a positive C_L is taken in the direction of $\vec{\omega} \times \vec{V_{rel}}$ for vorticity-induced lift and in the direction of $\vec{\Omega}_p \times \vec{V_{rel}}$ for particle-spin induced lift.

The different types of lift are often associated with the founding theories for each. For continuous-phase vorticity induced lift, there are three types: "Saffman lift" which is based on particles at $Re_p \ll 1$ subjected to a linear-shear flow [21], "Heron lift" which is based on particles at low-Re_p subjected to a vortex with solid-body rotation [22], and "Auton lift" which was presented as part of the AHP equation. In most flows, particles experience more of a "shearing" behavior than a "vortex" behavior. This behavior was confirmed for the present investigation by a conducting a direct numerical simulation of particles in a turbulent boundary layer using the methodology of [23]. The magnitude of Saffman and Heron lifts were computed and compared and it was observed that the former was many times larger than the latter.

Shear-induced lift The Saffman lift is based on the assumption of a particle exposed to creeping flow and a linear-shear velocity profile. In this situation a lift force is generated on the particle due to the difference in pressure exerted by the fluid on opposite sides of the particle (owing the different fluid velocities resulting from the velocity shear). Saffman's matched asymptotic expansion for the lift force is restricted to creeping flow conditions where

$$Re_p \ll Re_\omega^{1/2} \tag{28}$$

$$Re_\omega \equiv \frac{\|\vec{\omega}\| d_p^2}{\nu} \ll 1 \tag{29}$$

Further assuming $Re_p \ll Re_\omega^{1/2}$ gives, to leading-order,

$$F_{L,Saff} = 1.615 \mu \|\vec{V}_{rel}\| d_p^2 \sqrt{\frac{\|\vec{\omega}\|}{\nu}} \tag{30}$$

Note that Saffman lift can be written in lift-coefficient form as

$$C_{L,Saff} \equiv \frac{12.92}{\pi} \sqrt{\frac{\omega^*}{Re_p}} \tag{31}$$

Saffman noted that two higher-order terms also arise but that these are generally negligible in comparison, particularly for a freely-rotating particle at low-Re_p [24]. McLaughlin [25], extended Saffman's result to eliminate the restriction of $Re_p \ll Re_\omega^{1/2}$. This function was approximated by Mei [26] as

$$J^* \simeq 0.3 \left\{ 1 + \tanh\left[\frac{5}{2} \left(\log_{10} \sqrt{\frac{\omega^*}{Re_p}} + 0.191 \right) \right] \right\} \left\{ \frac{2}{3} + \tanh\left[6 \sqrt{\frac{\omega^*}{Re_p}} - 1.92 \right] \right\} \tag{32}$$

where $J^* \equiv C_{L,\omega}/C_{L,Saff}$. This expression was derived for small Reynolds numbers but Loth [15] found that this lift force is reasonable for $Re_p < 50$ and $\omega^* < 0.8$.

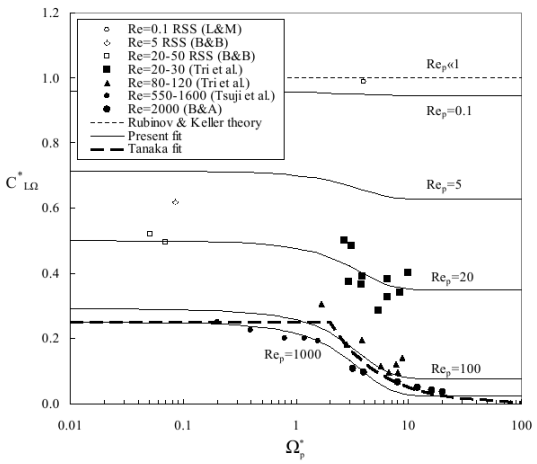

Figure 3. Spin lift force coefficient compared with small and intermediate Reynolds number ($Re_p < 2000$) compared to data of Tri et al. [29], Tsuji et al. [30], Barkla & Auchterlonie [31] (B&A), and resolved surface simulations (RSS) of Bagchi & Balachandar [32] (B&B) and Legendre & Magnaudet [9] (L&M).

Lift induced by particle rotation For small but finite Re_p, Rubinov & Keller [27] derived the analytic solution for spin-induced lift in the limit of small spin rates ($\Omega_p^* \ll 1$) for a solid sphere. Their analysis considers a velocity field which is a linear combination of the Oseen solution and that due to a rotating sphere in an otherwise stagnant fluid. Their expression can be generalized as:

$$\vec{F}_{L,\Omega_p} = \frac{\pi}{8} d_p^3 \rho_f \left(\vec{\Omega}_p \times \vec{V_{rel}}\right) C_{L,\Omega}^* \tag{33}$$

where $C_{L,\Omega}^* = 1$ for $Re_p \ll 1$. To include finite rotation rate and finite Reynolds number effects, an empirical correction can be given based on theory, experiments, and resolved-surface simulations (RSS) as

$$C_{L,\Omega}^* = 1 - \left\{0.675 + 0.15\left(1 + \tanh\left[0.28\left(\Omega_p^* - 2\right)\right]\right)\right\} * \tanh\left[0.18 Re_p^{1/2}\right] \tag{34}$$

This reverts to the theoretical value for $Re_p \ll 1$ and approximately to the Tanaka [28] fit for high Re_p as shown in Figure 3. This model is more robust than previous models which assume the lift coefficient is simply a constant, e.g. $C_{L,\Omega}^* = 0.4$ [29] or $C_{L,\Omega}^* = 0.55$ [32].

Combined shear-induced and rotation-induced lift To represent both the contribution of fluid vorticity and particle rotation to the particle lift force, one can consider summing the rotational and shear induced lift coefficients. Saffman [21] showed this to hold true for the theoretical particle spin lift of Rubinov & Keller combined with the first order shear-induced lift assuming creeping flow conditions and $\Omega_p^* \ll 1$. In this case, the combined lift coefficient (assuming spin and shear are both perpendicular to the relative velocity and yield a positive lift) is given by:

$$C_L = \frac{12.92}{\pi}\sqrt{\frac{\omega^*}{Re_p}} + \Omega_p^* \tag{35}$$

Bagchi & Balachandar [32] and others proposed that this simple linear combination could also be extended to Reynolds numbers, shear rates, and spin rates that were no longer much less than unity, i.e. the lift for combined fluid shear and particle spin can be given as

$$\vec{F}_L(\omega \neq 0, \Omega \neq 0) \approx \vec{F}_{L,\omega}(\omega \neq 0, \Omega_p = 0) + \vec{F}_{L,\Omega}(\omega = 0, \Omega_p \neq 0) \tag{36}$$

This assumption was found to be reasonable based on RSS results for ω^* and Ω_p^* values as high as 0.4 and Re_p values as high as 100 [32].

To employ the spin-induced lift for a torque-free particle, one must consider the equilibrium spin rate. For creeping flow, [33] noted that the rotation of the particle and surrounding fluid are balanced

$$\vec{\Omega}_{p,eq}^* = \frac{\vec{\omega}^*}{2} \tag{37}$$

Equilibrium is generally assumed for low density particles ($\rho_p \ll \rho_f$) because there is *no added mass effect*associated with the angular acceleration. However, it is often reasonable for drops and particles as well so long as the changes in relative particle rotation are of a time-scale that is long compared to the particle angular response time. To extend this to finite Re_p and finite Re_ω values, an empirical model (shown in Fig. 4) can be developed based on experimental data and resolved-surface simulations as

$$\Omega_{p,eq}^* = \frac{\omega^*}{2}(1 - 0.0075 Re_\omega)\left(1 - 0.062 Re_p^{1/2} - 0.001 Re_p\right) \tag{38}$$

This expression differs for that of [15] which used a different non-dimensionalization and had an error in the subscript but is superior to the fit by [34] which is also shown on the plot.

Noting that Eq. 38 does a reasonable job predicting the equilibrium spin rate for a range of conditions, it can be used along with the McLaughlin lift (Eq. 32) to define a lift coefficient appropriate for spherical particles which are solid or have a contaminated fluid interface at finite Reynolds numbers which are

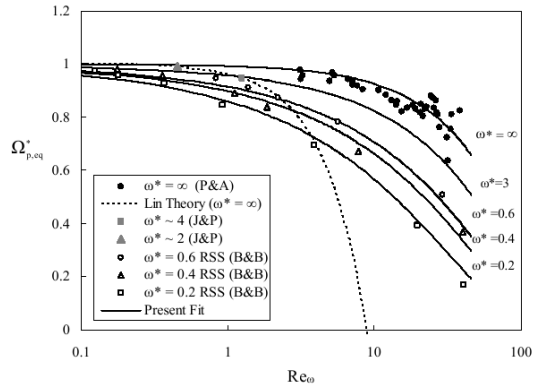

Figure 4. Equilibrium particle rotation rates based on data from Jeffrey & Pearson [35] and Poe & Acrivos [24] as well as resolved surface simulations (RSS) from Bagchi & Balachandar [32].

constantly in rotational equilibrium. To summarize, the lift of such spin-equilibrium particles at finite Reynolds numbers of up to $Re_p = 50$ can be given as

$$C_L = J^* \frac{12.92}{\pi} \sqrt{\frac{\omega^*}{Re_p}} + \Omega^*_{p,eq} C^*_{L,\Omega} \tag{39}$$

Equation of motion for finite-sized particles

The above point-force expressions in Section assumes weak spatial variations on the order of the particle scale. This lack of Faxen-type corrections for finite Reynolds numbers is consistent with almost all multiphase simulations for which the particle surface has not been resolved. In fact, such finite size corrections are typically avoided even in creeping flow conditions because few, if any, studies have investigated the impact of discretization on representing such corrections. The point-force assumption in turbulent flow formally requires $d_p \ll \lambda$ [36], where λ is the Kolmogorov length-scale. For example, consider a particle in a turbulent flow where one can show that for a Stokesian drag law, the particle diameter normalized by λ is proportional to Kolmogorov Stokes number (St_λ),

$$\left(\frac{d_p}{\lambda}\right)^2 = \frac{18}{\psi + C_M} St_\lambda \tag{40}$$

where $\psi = \rho_p/\rho_f$ and

$$\lambda = \left(\frac{\nu_f^3}{\varepsilon}\right)^{1/4} \qquad \text{and} \qquad St_\lambda = \frac{(\psi + C_M)\, d_p^2}{18\nu} \left(\frac{\varepsilon}{\nu}\right)^{1/2} \tag{41}$$

and where $\nu_f = \mu_f/\rho_f$. The above relation for a glass particle in a gas with $\psi = 1800$ suggests $St_\lambda \ll 100$ is appropriate for a conventional point-force approximation. However, an air bubble in water requires $St_\lambda \ll 1/36$ to satisfy this condition. Such a small Stokes number is effectively negligible in most cases such that the point-force method is only strictly valid for bubbles which are tracer particles! As such, an interesting bubble (i.e. one with appreciable inertia) will not, regardless of flow conditions, satisfy the point-force requirements and one is forced to seek a better technique.

The spatially-averaged method is based on an Eulerian representation of the continuous-phase flow and a Lagrangian description of the particle trajectories and velocities. Previous versions of this approach have employed a simple volume-average for the continuous-phase velocity within a filter-radius. In particular, a Heaviside weighting function ($\mathcal{H}$) can be specified as nonzero when the distance from the particle centroid (r) is within the filter-radius so that the continuous-phase velocity from all the nodes within this filter-radius are averaged:

$$\mathcal{H}(\vec{x}_j, \vec{x}_p) = \begin{cases} 1 & r \le a_z r_p \\ 0 & otherwise \end{cases} \tag{42}$$

$$\vec{V}_{f,avg} = \frac{\sum_{j=1}^{N_z} \vec{V}_f(\vec{x}_j)\, \mathcal{H}(\vec{x}_j, \vec{x}_p)}{\sum_{j=1}^{N_z} \mathcal{H}(\vec{x}_j, \vec{x}_p)} \tag{43}$$

where a_z is the non-dimensional filter radius. The relative particle velocity for drag and lift forces can then be obtained as $\vec{V}_{rel,avg} = \vec{V}_p - \vec{V}_{f,avg}$. Bagchi & Balachandar [37] investigated this weighting function with a_z values of 1.2 and 10 for a fixed solid particle in a turbulent flowfield. The spatially-averaged force results were compared to both resolved-surface force predictions and point-force predictions. In general, the spatially-averaged method compared reasonably well with the resolved-surface predictions for $d_p = 1.5\lambda$ with mean Re_p of 260. For larger particles with $d_p = 9.6\lambda$ with a mean Re_p of 600, the spatially-averaged method yielded poor correlations but at least gave the correct level of fluctuations, whereas the point-force gave large non-physical oscillations. Similar differences were found by Zeng et al. [38] in a turbulent boundary layer for $d_p = 14.3\lambda$ and a Re_p of about 300 for various a_z values. The Zeng et al. study also noted that effects of turbulence intensity, d^+, Re_p were significant but secondary to the effects of d_p/λ. A study of a clean bubble conducted by Merle et al. [39] for $d_p = 8\lambda$ with a mean Re_p of 500 found that a point-force model tended to overestimate the resolved-surface force fluctuations somewhat while a spatially-averaged expression with $a_z = 1$ tended to underestimate the fluctuations. Thus, previous spatial-averaging models show some promise but are largely empirical in design and have only been examined in the context of high Reynolds number particles. Another option, proposed

herein, is to develop a spatially-averaged technique based on theoretical considerations.

In the following, a distributed-force technique based on spatial-averaging is discussed. This new approach takes into account variations in the continuous-phase properties over the particle volume such that the length-scale (and corresponding Stokes number) restriction can be relaxed. This technique is developed for both low-Reynolds number and inviscid theoretical limits, followed by a generalized semi-empirical expression and discrete representations for computational implementation. This new approach is generally fourth-order accurate with respect to particle diameter such that much larger particles can be modeled than allowed by conventional point-force approaches.

Surface Force in Non-Uniform Flow at Low Reynolds Numbers

The quasi-steady drag force for general particle shapes was considered for a non-uniform continuous-phase velocity field by Brenner [40]. He used the reciprocal theorem to express the drag force at small Reynolds numbers in terms of the average continuous-phase velocity on the particle surface ($\vec{V}_{f,surf}$):

$$\vec{F}_D = -\frac{3\mu_f}{d_p} \oiint_{Ap} \left(\vec{V}_p - \vec{V}_f\right) d(A_p) = -3\mu_f d_p \left(\vec{V}_p - \vec{V}_{f,surf}\right) \tag{44}$$

where A_p is the particle surface and has a value of πd_p^2 for a spherical particle. It can be shown that the particle torque can be similarly related to the surface-averaged vorticity at small Reynolds numbers. Thus, the spin-equilibrium of Eq. 38 should also be based on surface averages of vorticity and continuous-phase velocity. For a spherical particle surface, a Taylor series can be used to replace the surface average of a quantity q with its value and its even-numbered derivatives evaluated at the particle center [41] as

$$\oiint_{A_p} q dA_p = A_p \left[q_{@p} + \frac{d_p^2}{24} \left(\nabla^2 q\right)_{@p} + \frac{d_p^4}{1920} \left(\nabla^4 q\right)_{@p} + ... \right] \tag{45}$$

For Stokes flow, $\nabla^4 V_f \equiv 0$ so that the drag force can then be expressed in terms of the conventional Faxen corrections given by the MR equation of motion (Eq. 5):

$$\begin{aligned} \vec{F}_D &= -3\mu_f d_p \left(\vec{V}_p - \vec{V}_{f,surf}\right) \\ &= -3\mu_f d_p \left[\vec{V}_p - \vec{V}_{f,@p} - \frac{d_p^2}{24}\left(\nabla^2 \vec{V}_f\right)_{@p}\right] \\ &= -3\mu_f d_p \left[\vec{V}_{rel} - \frac{d_p^2}{24}\left(\nabla^2 \vec{V}_f\right)_{@p}\right] \end{aligned} \tag{46}$$

Note that the history force of MR includes a similar Faxen correction (Eq. 8) also consistent with $\vec{V}_{f,surf}$. In summary, the low Reynolds number drag and surface torque in a non-uniform flow arise from a surface average of the continuous-phase velocity and vorticity.

The reciprocal theorem was also used by Lovalenti & Brady [42] to extend the surface forces to incorporate conditions of small but finite Reynolds numbers (for which the Oseen correction is valid and for which Saffman lift is valid). They showed that the above Faxen corrections are still appropriate for a solid particle but that the correction should be reduced for a fluid particle with finite viscosity as:

$$\begin{aligned} \vec{F}_D = -3\mu_f d_p \Bigg[&\left(\frac{3\mu_p + 2\mu_f}{3\mu_p + 3\mu_f}\right)\left(\vec{V}_p - \vec{V}_{f,@p}\right) \\ &- \frac{d_p^2}{24}\left(\frac{3\mu_p}{3\mu_p + 2\mu_f}\right)\left(\nabla^2 \vec{V}_f\right)_{@p}\Bigg] \end{aligned} \tag{47}$$

where μ_p is the particle viscosity. The right-hand-side in the limit of a clean bubble with negligible viscosity in uniform flow is consistent with the Hadamard-Rybczynski solution, i.e. $-2\mu_f d_p(\vec{V}_P - \vec{V}_{f,@p})$. As such, the drag force of a clean bubble should employ a centroid-based fluid velocity and not a surface-average, which is qualitatively consistent with the results of Merle *et al.*[39].

For small but finite Reynolds numbers, Lovalenti & Brady [42] considered unsteady conditions and showed that the fluid stress and added mass force for a solid sphere can be written in terms of volume-based averages of the fluid accelerations:

$$\begin{aligned} \vec{F}_{SG} &= \rho_f \iiint_{\forall_p} \left(\frac{D\vec{V}_f}{Dt} - \vec{g}\right) d\forall_p \\ &= \rho_f \forall_p \left[\left(\frac{D\vec{V}_f}{Dt}\right)_{vol} - \vec{g}\right] \end{aligned} \tag{48}$$

$$\begin{aligned} \vec{F}_{AM} &= -C_M \rho_f \iiint_{\forall_p} \frac{d\left(\vec{V}_p - \vec{V}_f\right)}{dt} d\forall_p \\ &= -C_M \rho_f \forall_p \left[\frac{d\vec{V}_p}{dt} - \left(\frac{d\vec{V}_f}{dt}\right)_{vol}\right] \\ &\approx -C_M \rho_f \forall_p \left[\frac{d\vec{V}_p}{dt} - \left(\frac{D\vec{V}_f}{Dt}\right)_{vol}\right] \end{aligned} \tag{49}$$

The approximation of the particle Lagrangian time-derivative as the continuous-phase Lagrangian time-derivative is appropriate in the limit of small Reynolds numbers [3]. As such, the fluid stress and added mass forces for a solid particle in a non-uniform

flow arise directly from a volume average. As with the drag force, adjustments are required for an uncontaminated fluid particle with finite viscosity [42].

By applying two additional assumptions, the above volume-averaged result for added mass can be simplified to yield conventional the Faxen correction. The first of these assumptions is to swap the differentiation and the spatial-averaging as follows:

$$\left(\frac{D\vec{V}_f}{Dt}\right)_{vol} = \left(\frac{\partial\vec{V}_f}{\partial t}\right)_{vol} + \left[\vec{V}_f\cdot\nabla\vec{V}_f\right]_{vol} \approx \frac{\partial\vec{V}_{vol}}{\partial t} + \vec{V}_{f,vol}\cdot\nabla\vec{V}_{f,vol} \approx \frac{D\vec{V}_{f,vol}}{Dt} \quad (50)$$

This is often a reasonable approximation because the fluid-acceleration gradients are typically weak since they are higher-order than the fluid-velocity gradients. Next, a Taylor series can be used to replace the volume average of a quantity q in terms of properties at the centroid if the particle is spherical:

$$\iiint_{\forall_p} q d\forall_p = \forall_p\left[q_{@p} + \frac{d^2}{40}\left(\nabla^2 q\right)_{@p} + \frac{d^4}{4480}\left(\nabla^4 q\right)_{@p} + ...\right] \quad (51)$$

Making the second assumption of creeping flow which yields Faxen corrections for the fluid stress and added mass forces:

$$\vec{F}_{SG} = \rho_f\forall_p\frac{D}{Dt}\left[\vec{V}_{f,@p} + \frac{d^2}{40}\left(\nabla^2\vec{V}_f\right)_{@p}\right] - \rho_f\forall_p\vec{g} \quad (52)$$

$$\vec{F}_{AM} = -C_M\rho_f\forall_p\frac{d}{dt}\left[\vec{V}_p - \vec{V}_{f,@p} - \frac{d^2}{40}\left(\nabla^2\vec{V}_f\right)_{@p}\right] \quad (53)$$

This added-mass correction is equal to that of MR (Eq. 7) but the correction for the fluid-stress force was not included by MR (Eq. 6) since they assumed that the fluid stress was approximately constant in the vicinity of the sphere (which is a generally reasonable assumption). Thus, the conventional Faxen corrections are consistent with, but actually less accurate than, the volume-average expressions of Eqs. 52 & 53 for finite Reynolds numbers.

The lift in a non-uniform flow at small Reynolds numbers was discussed by Saffman [21], who found a solution for a linear shear field. He also discussed the potential extension to Poiseuille flow with non-uniform shear but found the problem to be "intractable". Because of this, no Faxen-type corrections have been previously derived for lift. However, the Saffman lift derivation is based on a surface integral of the square root of the vorticity, so that the lift force for small but finite Reynolds numbers can be written as

$$\vec{F}_{L,Saff} = 1.615\rho_f d_p^2\sqrt{\frac{\nu_f}{\omega_{shear,surf}}}\left(\vec{\omega}_{shear,surf}\times\left(\vec{V}_p - \vec{V}_{f,surf}\right)\right) + O\left(d_p^3\frac{\nabla\omega_{shear,surf}}{\sqrt{\omega_{shear,surf}}}, d_p^4\frac{\nabla^2\omega_{shear,surf}}{\sqrt{\omega_{shear,surf}}}\right) \quad (54)$$

The third-order truncation term may be expected to be small owing to symmetry (as found for other surface and volume forces) as is the fourth-order truncation term since $\nabla^2\omega \equiv 0$ for Stokes flow. However, a better understanding of these truncation terms probably requires numerical experiments in flows with varying vorticity.

Surface Force in Non-Uniform Inviscid Flow

The AHP expressions for surface include fluid-stress, added-mass and lift forces. Recall the fluid-stress force is simply the continuous-phase stresses on the particle surface in the absence of the particle disturbances. This can be transformed to a volume integral based by employing Gauss's theorem. As such, the inviscid fluid-stress force is equal to the low Reynolds number volume-averaged form of Eq. 49. This is not surprising force since this derivation is independent of particle Reynolds number.

The added mass for a quadratically varying shear flow is difficult to assess as there is no closed-form inviscid solution for a solid sphere. However, one may reasonably argue that it should be the same as that in Eq. 49, where the creeping flow result for a solid particle in a non-uniform flow arises directly from a volume average. This is because the added mass force for both uniform flow and linear shear is the same at both creeping flow and inviscid flow and is independent of particle Reynolds number for intermediate conditions. As such, the above volume-averages are expected to be third-order accurate in particle diameter for solid spherical surfaces in quadratically-varying velocity fields.

The only other remaining inviscid force to consider is the Auton lift force. For constant vorticity, the inviscid lift is the same for pure rotational flow as it is for linear shear flow (which includes strain). If the flow does not have any strain so that it is in pure rotation, the vorticity does not affect the zero-penetration surface boundary conditions and so can vary radially. Neglecting the time derivatives, assuming weak gradients in the vorticity, and employing the linearization for surface pressure of [6] allows the lift force to be expressed as:

$$\vec{F}_L = \frac{1}{2}\rho_f\forall_p\left[\vec{\omega}_{vortex,surf}\times\left(\vec{V}_p - \vec{V}_{f,surf}\right)\right] \quad (55)$$

Since the inviscid lift derivation is not straightforward for shear flow with non-uniform vorticity as discussed above, truncation

terms are needed to generalize the lift force:

$$\vec{F}_L = \frac{1}{2}\rho_f \forall_p \left[\vec{\omega}_{surf} \times \left(\vec{V}_p - \vec{V}_{f,surf}\right)\right] \quad (56)$$

$$+ O\left(d_p^3 \frac{\nabla \omega_{surf}}{\sqrt{\omega_{surf}}},\, d_p^4 \frac{\nabla^4 \omega_{surf}}{\sqrt{\omega_{surf}}}\right) \quad (57)$$

Quantitative assessment for the truncation terms in the above expression may require numerical experiments in such flows. However, the impact of vorticity gradients may be weak based on the results of Merle et. al. [39].

Generalized Particle Surface Force in Non-Uniform Flow

Based on the above, a semi-empirical expression for a spherical particle which is solid or a contaminated fluid at finite Reynolds number and non-uniform unsteady flows can be constructed:

$$\begin{aligned}\vec{F}_{surf} = & -3\pi d_p \mu_f \left(\vec{V}_p - \vec{V}_{f,surf}\right)\left(1 + 0.15 Re_{p,surf}^{0.687}\right) \\ & -\rho_f \forall_p \vec{g} + \rho_f \forall_p \left[(1+C_M)\left(\frac{D\vec{V}_f}{Dt}\right)_{vol} - C_M \frac{d\vec{V}_p}{dt}\right] \\ & -\frac{3}{2} d_p^2 \sqrt{\pi \rho_f \mu_f}\left[\int_0^t K\left(t-\tau, Re_{p,surf}\right) \frac{d\left(\vec{V}_p - \vec{V}_{f,surf}\right)}{d\tau} d\tau\right] \\ & +\vec{F}_L\left(\vec{V}_{f,surf}, \vec{\omega}_{surf}\right) \end{aligned} \quad (58)$$

This form is limited to Re_p of 50 or less and spin-equilibrium if one employs the empirical corrections for the history force and lift force discussed in Sections and but the relative velocity in the Reynolds number should be replaced with a surface-average. However, it should be noted that the non-uniform effects have only been strictly derived for limits of small Reynolds number and inviscid conditions for certain sets of these forces. Similar corrections can be applied to the particle energy ODE with heat and mass transfer since [43] shows that it employs a Laplacian correction for the continuous-phase temperature analogous to the Faxen correction for the momentum transfer. As such, a "Michaelides correction" for surface heat transfer can be represented by employing a surface-averaged fluid temperature while the unhindered thermal stress can be described in terms of a volume-averaged fluid temperature.

Discrete Surface- and Volume-Averages

For the discrete form of the surface and volume-averages, it is straightforward to use sampling at particular locations. The surface-average can employ six sampling points to capture the gradients in all three directions. If the surface sampling points are denoted by (x_s, y_s, z_s), they can be set based on left/right, top/bottom and front/back, i.e. $x_s = x_p \pm r_p$, $y_s = y_p \pm r_p$, and $z_s = z_p \pm r_p$. The surface-averaged velocity is then

$$\vec{V}_{f,surf} = \frac{1}{A_p}\iint_{A_p} \vec{V}_f dA_p \approx \frac{1}{6}\sum_{i=1}^{6} \vec{V}_{f,s} \equiv \vec{V}_{f,surf,\Sigma} \quad (59)$$

A similar six-point approach for the surface-averaged vorticity can be used for lift. To show that this sampling gives a reasonable surface-average description, consider an unhindered flow-field with a polynomial variation in horizontal shear and a uniform vertical velocity:

$$\begin{aligned}\vec{V}_f = u_{f,@p}\Bigg[1 + \frac{y}{l_1} + \left(\frac{y}{l_2}\right)^2 + \left(\frac{y}{l_3}\right)^3 \\ + \left(\frac{y}{l_4}\right)^4 + \left(\frac{y}{l_5}\right)^5\Bigg]\hat{\imath} + v_{f,@p}\hat{\jmath}\end{aligned} \quad (60)$$

In this expression l_1, l_2, etc. are length-scale constants which are inversely proportional to the velocity derivatives which are first-order, second-order, etc. Substitution into Eq. 59 yields:

$$\vec{V}_{f,surf,\Sigma} = \vec{V}_{f,@p} + \frac{d_p^2}{24}\left(\nabla^2 \vec{V}_f\right)_{@p} + \frac{d^4}{1152}\left(\nabla^4 \vec{V}_f\right)_{@p} \quad (61)$$

For Stokes flow with $\nabla^4 \vec{V}_f \equiv 0$, the discrete distributed-force method is identical to the exact solution and the Faxen correction even if the sampling points on the sphere are rotated. In contrast, the conventional point-force (using only $\vec{V}_{f,@p}$) yields a second-order error which increases with the particle diameter and flow gradient as shown in Figure 5. For non-Stokesian flows with a finite $\nabla^4 \vec{V}_f$, the discrete average (Eq. 61) is fourth-order accurate in diameter compared to both the exact solution (Eq. 45) and the Faxen correction (Eq. 44) and substantially more accurate than a conventional point-force (Figure 5b).

For the volume-averaged fluid acceleration, it is convenient and computationally efficient to use the same six surface sampling points along with an additional sampling point at the particle centroid ($\vec{x}_p$). This combination can be optimized using a fourth-order accurate Simpson's rule for spherical integration to

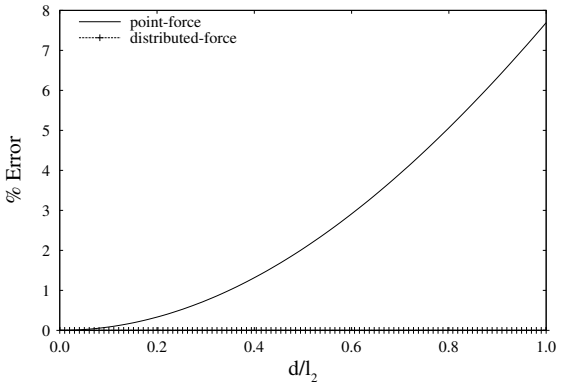

a) quadratic variation

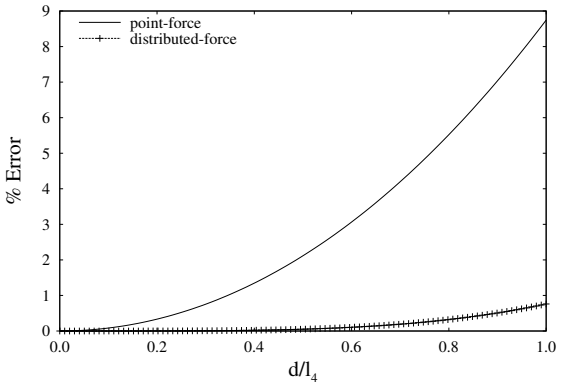

b) quartic variation

Figure 5. Surface-averaged horizontal force error for point-force and distributed-force approaches for a stationary particle subjected to polynomial shear flows of quadratic and quartic variation.

approximate the volume average:

$$\left(\frac{D\vec{V}_f}{Dt}\right)_{vol} = \frac{1}{\forall_p}\iiint_{\forall_p}\left(\frac{D\vec{V}_f}{Dt}\right)d\forall_p \approx \frac{3}{5}\left[\frac{1}{6}\sum_{i=1}^{6}\left(\frac{D\vec{V}_f}{Dt}\right)_{s,i}\right] + \frac{2}{5}\left(\frac{D\vec{V}_f}{Dt}\right)_{@p} = \left(\frac{D\vec{V}_f}{Dt}\right)_{vol,\Sigma} \quad (62)$$

Application of this discrete approximation to the steady velocity field of Eq. 60, for which

$$\left(\frac{D\vec{V}_f}{Dt}\right) = v_{f,@p}\frac{\partial u}{\partial y}\hat{i} \quad (63)$$

yields:

$$\left(\frac{D\vec{V}_f}{Dt}\right)_{vol,\Sigma} = \left(\frac{D\vec{V}_f}{Dt}\right)_{@p} + \frac{d_p^2}{40}\left[\nabla^2\left(\frac{D\vec{V}_f}{Dt}\right)\right]_{@p} + \frac{d^4}{1920}\left[\nabla^4\left(\frac{D\vec{V}_f}{Dt}\right)\right]_{@p} \quad (64)$$

Again, the discrete sampling method and the Faxen correction (Eq. 49) are exact for Stokes flow conditions and (based on Eq. 51) are fourth-order accurate with respect to particle diameter for non-Stokesian flows. Comparisons are made in Figure 6 of the point-force and distributed force error compared to the analytical solution for both the complete velocity field described by Eq. 60 and truncated velocity field which neglects the 4^{th} and 5^{th}-order terms. Figure 6 shows that the distributed force formulation is exact for the cubic variation (as expected) while the point-force expression admits $\sim 4.5\%$ error at $d/l_3 = 1$. The distributed force admits errors on the higher-order variation but is still $\sim 5x$ more accurate than the point-force formulation at $d/l_5 = 1$.

Sinusoidal Shear Flow

To investigate the discrete distributed-force approach in the context of a flowfield more relevant to turbulence, a sinusoidal shear layer is considered whose spatial variation is characterized by a length scale and a velocity amplitude:

$$\vec{V}_f = u_l \sin\left(\frac{2\pi y}{l}\right)\hat{\imath} + v_{y@p}\hat{\jmath} \quad (65)$$

The horizontal velocities for the point-force, exact and discrete surface-averages are given by:

$$u_{@p} = u_l \sin\left(\frac{2\pi y_p}{l}\right) \quad (66)$$

$$u_{surf} = u_l \sin\left(\frac{2\pi y_p}{l}\right)\left[1 - \frac{(\pi d_p)^2}{6} + \frac{(\pi d_p)^4}{320}\right] \quad (67)$$

$$u_{surf,\Sigma} = u_l \sin\left(\frac{2\pi y_p}{l}\right)\left[1 - \frac{(\pi d_p)^2}{6} + \frac{(\pi d_p)^4}{72}\right] \quad (68)$$

Again, the point-force method is second-order accurate in particle diameter and the discrete method is fourth-order accurate (a result which can also be shown to be true for a volume average). A spatially-integrated velocity difference from the exact solution may be obtained by considering all particle positions in the sine wave (equivalent to the particle moving at a constant vertical

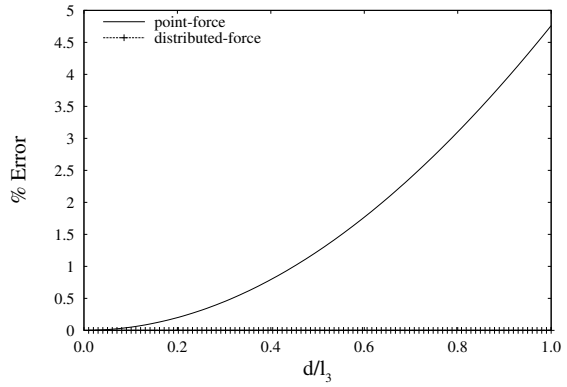

a) cubic variation

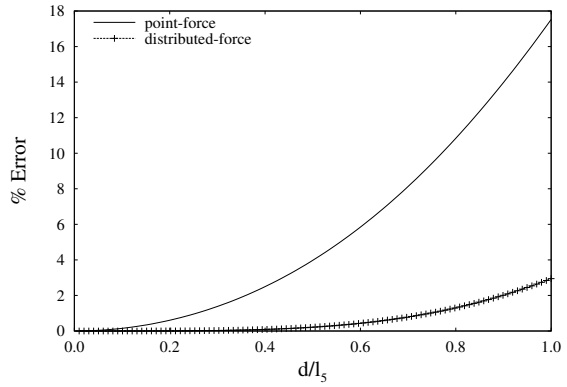

b) quintic variation

Figure 6. Volume-averaged error for point-force and distributed-force formulations for a stationary particle subjected to a polynomial shear flow velocity variation that is: a) cubic and b) quintic.

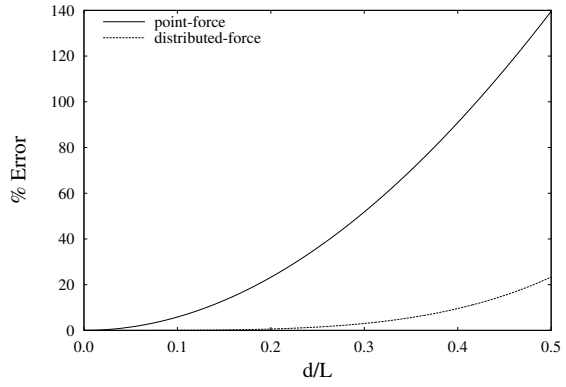

a) surface-average

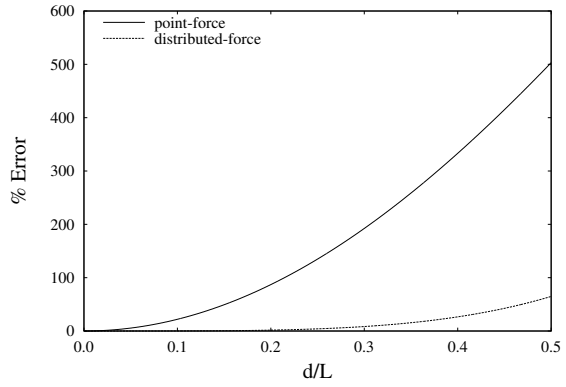

b) volume-average

Figure 7. Horizontal force errors for point-force and distributed-force representations for a particle subjected to a sinusoidal shear flow based on: a) surface-average and b) volume-average.

speed through one wavelength). The error in the point-force expression for a surface-averaged horizontal force (e.g., drag force) can be expressed as:

$$\text{error} = [u_{surf} - u_{@p}]_{rms} = \left[\frac{1}{2\pi l}\int_0^{2\pi l}[u_{surf} - u_{@p}]^2\, dy_p\right]^{1/2} \tag{69}$$

The integrated errors are shown in Figure 7a, for which an increase in particle diameter with respect to the wavelength results in a substantial increase for the point-force approach. For the distributed-force approach, the errors are generally an order of magnitude smaller. A similar result is found volume-averaged forces of added mass and fluid-stress (based on the volume-averaged fluid acceleration) as shown in Figure 7b.

Based on the above analysis, some comments may be made on possible implications for turbulent flow conditions. Consider a particle falling at a speed approximately equal to its terminal velocity which approximately follows Stokes drag law. Assume that the flow is composed of a range of wavelengths (l) where each is associated with a velocity fluctuation amplitude (u_l) all superimposed upon a mean velocity ($\bar{u}$). The errors in the drag point-force method for a given wavelength will be small if the turbulence is weak ($u_l \ll \bar{u}$) or if the particle is small ($d_p \ll l$). For finite particle sizes with $d_p < l$, the relative drag force error is of order $(u_l d_p)/(\bar{u}l)^2$. Since the turbulence intensity in the inertial sub-range varies only weakly with wavelength, $u_l \sim (\varepsilon l)^{1/3}$, the largest errors will occur as $d_p \to l$. However, once the particles become larger ($d_p > l$), the wavelengths become sub-scale and so that variations across the particle only increase weakly, i.e. with $l^{1/3}$. As such, the point-force errors can be primarily related to wavelengths on the order of the particle size. In turbulence, this indicates that the errors will scale with $u'_{rms}/(u'_{rms} + \bar{u})$ for particle sizes larger than the Kolmogorov scale ($d_p > \lambda$) where u'_{rms} is the turbulence intensity and is proportional to u_l. This result is qualitatively consistent with resolved-surface simulations of [44] for $d = 2\lambda$ and $Re_p \sim 5 - 20$ who noted that the point-

force errors (primarily related to drag) were as large as 30% and scaled with turbulence intensity. The trends shown in Figure 7 indicate that the errors for the distributed force may be an order of magnitude smaller than that for the point-force, but investigation with resolved-surface simulations and/or experiments are needed before this can be confirmed for turbulent flow or even simple polynomial or sinusoidal shear flows. Furthermore, the proposed distributed force expressions are developed based on theoretical limits for idealized conditions of a single spherical particle and may only be approximate for lift and do not include effects of fluid strain [45].

Conclusion

The effect of finite particle Reynolds number was first considered for particles subjected to weak spatial gradients (compared to the particle size) such that the convetional point-force approximation remains valid. In addition to revisiting the conventional surface force expressions for quasi-steady drag, lift, added mass and fluid stress, an efficient expression for the history force is described along with a spin-equilibrium lift coefficient. These expressions are expected to be reasonable up to a particle Reynolds number of 50.

In the second part of this study, the effect of finite particle size was considered to extend the equation of motion to particle sizes in which the point-force treatment is not valid. To this end, a spatially-averaged method consistent with known theoretical limits for the particle surface force was developed to incorporate finite particle size effects. For a spherical particle with a no-slip surface, it results in a surface-average for the quasi-steady drag, history and lift forces and a volume-average for the fluid-stress and added-mass forces. The theoretical justification for these averages is discussed for both low Reynolds number and inviscid limits, and this is employed to put forth a generalized semi-empirical expression. It was shown that the surface-average can be obtained with simple six-point (front/back, top/bottom and left/right) discrete average while the volume-average can be constructed using a seven-point average based on the particle centroid and a spherical Simpson integration rule. These discrete averages correctly tend to the MR and AHP point–force expressions, including the Faxen corrections. Furthermore, they are fourth-order accurate for simple polynomial and sinusoidal shear flows and significantly more accurate than point-force analog. However, resolved-surface or experimental studies are needed to determine the robustness and limits of the proposed spatial-averaged approach in terms of both flow complexity and particle Reynolds number, especially for lift force where theoretical expressions are difficult to obtain even in the case of simple flow-fields.

References

[1] Stokes, G. G., 1851. "On the effect of the inertial friction of fluids on the motion of pendulums". *Trans. Cambr. Phil. Soc.,* ***9***, pp. 8–106.

[2] Maxey, M. R., and Riley, J. J., 1983. "Equation of motion for a small rigid sphere in a non-uniform flow". *Phys. Fluids,* ***26***, pp. 883–889.

[3] Maxey, M. R., 1993. "Equation of motion for a small rigid sphere in a non-uniform or unsteady flow". *ASME/FED Gas-Solid Flows,* ***166***, pp. 57–62.

[4] Faxen, H., 1922. "The resistance against the movement of a rigour sphere in viscous fluids, which is embedded between two parallel layered barriers". *Annalen Der Physik,* ***68***, pp. 89–119.

[5] Auton, T. R., 1987. "The lift force on a spherical body in a rotational flow". *J. Fluid Mech.,* ***183***, pp. 199–218.

[6] Auton, T. R., Hunt, J. C. R., and Prud'Homme, M., 1988. "The force exerted on a body in inviscid unsteady non-uniform rotational flow". *J. Fluid Mech.,* ***197***, pp. 241–257.

[7] Bataille, J., Lance, M., and Marie, J. L., 1991. "Some aspects of the modeling of bubbly flows". In *Phase-Interface Phenomena in Multiphase Flow*, G. F. Hewitt, F. Mayinger, and J. R. Riznic, eds. Hemisphere Publishing Corporation.

[8] Kim, I., Elghobashi, S., and Sirignano, W. B., 1998. "On the equation for spherical- particle motion: effect of reynolds and acceleration numbers". *J. Fluid Mech.,* ***367***, pp. 221–253.

[9] Legendre, D., and Magnaudet, J., 1998. "Lift force on a bubble in a viscous linear shear flow". *J. Fluid Mech.,* ***368***, pp. 81–126.

[10] Mei, R., and Klausner, J. F., 1992. "Unsteady force on a spherical bubble with finite reynolds number with small fluctuations in the free-stream velocity". *Phys. Fluids A,* ***4***, pp. 63–70.

[11] Mei, R., and Klausner, J. F., 1994. "Shear lift force on spherical bubbles". *Int. J. Heat and Fluid Flow,* ***15***, pp. 62–65.

[12] Mei, R., Lawrence, C. J., and Adrian, R. J., 1991. "Unsteady drag on a sphere at finite reynolds number with small fluctuations in the free-stream velocity". *J. Fluid Mech.,* ***233***, pp. 613–631.

[13] Wakaba, L. V., and Balachandar, S., 2007. "History force on a sphere in a weak linear shear flow". *Int. J. Heat and Fluid Flow,* ***31***, pp. 996–1014.

[14] Odar, F., and Hamilton, W. S., 1964. "Forces on a sphere accelerating in a viscous fluid". *J. Fluid Mech.,* ***18***, pp. 302–314.

[15] Loth, E., 2008. "Lift of a spherical particle subject to vorticity and/or spin". *AIAA J.,* ***46***, pp. 801–809.

[16] Schiller, L., and Naumann, A. Z., 1933. "Über die grundlegenden Berechungen bei der Schwerkraftaufbere-

itung". *Ver. Deut. Ing,* ***77***, pp. 318–320.
[17] Basset, A. B., 1888. "On the motion of a sphere in a viscous liquid". *Phil. Trans. R. Soc. London,* ***179A***, pp. 43–63.
[18] Mei, R., and Adrian, R. J., 1992. "Flow past a sphere with an oscillation in the free-stream and unsteady drag at finite reynolds number". *J. Fluid Mech.,* ***237***, pp. 323–341.
[19] Dorgan, A. J., and Loth, E., 2007. "Efficient calculation of the history force at finite reynolds numbers". *Intl. J. Multiphase Flow,* ***33***, pp. 833–848.
[20] Moorman, R. W., 1955. "Motion of a spherical particle in the accelerated portion of free-fall". PhD thesis, University of Iowa.
[21] Saffman, P. G., 1965. "The lift on a sphere in slow shear flow". *J. Fluid Mech.,* ***22***, pp. 385–400. Corrigendum, 1968. 31, 624.
[22] Heron, I., Davis, S., and Bretherton, F., 1975. "On the sedimentation of a sphere in a centrifuge". *J. Fluid Mech.,* ***68***, pp. 209–234.
[23] Dorgan, A. J., Loth, E., Bocksell, T. L., and Yeung, P. K., 2005. "Boundary layer dispersion of near-wall injected particles of various inertias". *AIAA J.,* ***43***, pp. 1537–1548.
[24] Poe, G. G., and Acrivos, A., 1975. "Closed-streamline flows past rotating single cylinders and spheres: Inertia effects". *J. Fluid Mech.,* ***72***, pp. 605–623.
[25] McLaughlin, J. B., 1991. "Inertial migration of a small sphere in linear shear flows". *J. Fluid Mech.,* ***224***, pp. 261–274.
[26] Mei, R., 1992. "An approximate expression for shear lift force on a spherical particle at a finite reynolds number". *Intl. J. Multiphase Flow,* ***18***, pp. 145–147.
[27] Rubinov, S. I., and Keller, J. B., 1961. "The transverse force on spinning spheres moving in a viscous liquid". *J. Fluid Mech.,* ***11***, pp. 3447–3459.
[28] Tanaka, T., Yonemura, S., and Tsuji, Y., 1990. "Experiments of fluid forces on a rotating sphere and spheroid". In Proc. 2nd KSME-JSME Fluids Engr. Conf.
[29] Tri, B. D., Oesterle, B., and Deneu, F., 1990. "Premiers resultants sur la portance d'une sphere en rotation aux nombres de reynolds intermediaies". *C. R. Acad. Sci. Ser. II: Mec. Phys. Chim. Sci Terre Universe,* ***311***, p. 27.
[30] Tsuji, Y., Morikawa, Y., and Mizuno, O., 1985. "Experimental measurements of the magnus force on a rotating sphere at low reynolds numbers". *J. Fluids Engr.,* ***107***, pp. 484–488.
[31] Barkla, H. M., and AuchterLonie, L. J., 1971. "The Magnus or Robins effect on rotating spheres". *J. Fluid Mech.,* ***47***, pp. 437–448.
[32] Bagchi, P., and Balachandar, S., 2002. "Effect of free rotation on motion of a solid sphere". *Phys Fluids,* ***14***, pp. 2719–2737.
[33] Happel, J., and Brenner, H., 1973. *Low Reynolds Number Hydrodynamics*. Noordhoff.
[34] Lin, C. J., Perry, J. H., and Scholwater, W. R., 1970. "Simple shear flow round a rigid sphere: Inertial effects and suspension rheology". *J. Fluid Mech.,* ***44***, pp. 1–17.
[35] Jeffrey, R. C., and Pearson, J. R. A., 1965. "Particle motion in a laminar vertical tube flow". *J. Fluid Mech.,* ***22***, pp. 721–735.
[36] Elghobashi, S., 1994. "On predicting particle-laden turbulent flows". *Applied Scientific Research,* ***52***, pp. 309–329.
[37] Bagchi, P., and Balachandar, S., 2003. "Effect of turbulence on the drag and lift of a particle". *Phys Fluids,* ***15***(11), pp. 3496–3513.
[38] Zeng, L., Balachandar, S., and Najjar, F., 2008. "Interactions of a stationary finite-sized particle with wall turbulence". *J. Fluid Mech.,* ***594***, pp. 271–305.
[39] Merle, A., Legendre, D., and Magnaudet, J., 2005. "Forces on a high-reynolds-number spherical bubble in a turbulent flow". *J. Fluid Mech.,* ***532***, pp. 53–62.
[40] Brenner, H., 1964. "The Stokes resistasnce of an arbitrary particle–IV arbitrary fields of flow". *Chemical Engineering Science,* ***19***, pp. 703–727.
[41] Hobson, E. W., 1931. *The Theory of Spherical and Ellipsoidal Harmonics*. Cambridge Univ. Press, republished 1955 by Chelsea Publishing Comp., New York.
[42] Lovalenti, P. M., and Brady, J. F., 1993. "The force on a sphere in a uniform flow with small-amplitude oscillations at finite reynolds number". *J. Fluid Mech.,* ***256***, pp. 607–614.
[43] Michaelides, E., 2003. "Hydrodynamic force and heat/mass transfer from particles, bubbles and drops–The Freeman Scholar Lecture". *J. Fluids Eng.,* ***125***, pp. 209–238.
[44] Burton, T. M., and Eaton, J. K., 2005. "Fully resolved simulations of particle-turbulence interaction". *J. Fluid Mech.,* ***545***, pp. 67–111.
[45] Bagchi, P., and Balachandar, S., 2002. "Steady planar straining flow past a rigid sphere at moderate reynolds number". *J. Fluid Mech.,* ***466***, pp. 365–407.